Chemical Science

ROYAL SOCIETY OF CHEMISTRY

EDGE ARTICLE

View Article Online
View Journal | View Issue

Cite this: *Chem. Sci.*, 2023, **14**, 6237

All publication charges for this article have been paid for by the Royal Society of Chemistry

Received 14th February 2023
Accepted 14th May 2023

DOI: 10.1039/d3sc00828b

rsc.li/chemical-science

Light-regulating chirality of metallacages featuring dithienylethene switches†

Shaomeng Guo,‡ Mengqi Li,‡ Honglong Hu, Ting Xu, Hancheng Xi and Wei-Hong Zhu *

Dynamic chiral superstructures are of vital importance for understanding the organization and function of chirality in biological systems. However, achieving high conversion efficiency for photoswitches in nanoconfined architectures remains challenging but fascinating. Herein, we report a series of dynamic chiral photoswitches based on supramolecular metallacages through the coordination-driven self-assembly of dithienylethene (DTE) units and octahedral zinc ions, thereby successfully achieving an ultrahigh photoconversion yield of 91.3% in nanosized cavities with a stepwise isomerization mechanism. Interestingly, the chiral inequality phenomenon is observed in metallacages, resulting from the intrinsic photoresponsive chirality in the closed form of the dithienylethene unit. Upon hierarchical organization, we establish a dynamic chiral system at the supramolecular level, featuring chiral transfer, amplification, induction, and manipulation. This study provides an intriguing idea to simplify and understand chiral science.

Introduction

Supramolecular chirality plays a pivotal role in biological systems, asymmetric catalysis, and materials science.[1–8] Understanding and manipulating the organization and function of homochirality in biochemistry and pharmacology are fascinating but challenging endeavours.[9–11] Photochromic dithienylethene (DTE) derivatives, an ideal class of photoswitches, can undergo a reversible transformation between the open state and closed state triggered by light, along with changes in optical and electronic properties.[12–19] Their distinctive optical performances together with their excellent thermostability afford them a promising candidate in supramolecular systems,[20–31] liquid crystal superstructures,[32–34] and super-resolution imaging.[35–37] Introducing photoresponsive DTE units into chiral systems is a significant and feasible strategy to construct dynamic chiral systems for mimicking and investigating life chirality.[38,39] However, for chiral nanoconfined frameworks, achieving high photoconversion efficiency in nanosized cavities still remains a formidable challenge.[40,41]

Metal-coordination self-assembly is one of the most stable and flexible synthetic strategies to construct supramolecular architectures, in which coordination assemblies can be well organized while simultaneously allowing precise control over the size, shape, and functionality.[42–56] Therefore, the fabrication of chiral DTE supramolecular metallacages *via* the coordination-driven self-assembly strategy, featuring intrinsic chiral responsive functions, may afford a fascinating dynamic chiral platform. Herein, we report a series of chiral metallacages, namely the open form (*R*/*S*)-*o*-**cage** and the closed form (*R*/*S*)-*c*-**cage**, fabricated by coordination-driven self-assembly of DTE units, chiral amines, and zinc ions (Fig. 1). Given the flexibility of building blocks and the stability of frameworks, we employed relatively rigid DTE units to build up frameworks while not restricting the isomerization performance, allowing for not only the transformation of molecular geometry but also the chirality of self-assembled metallacages. In addition, traditional DTE systems always lose their intrinsic chirality due to rapidly interconvertible helical structures.[13,57,58] Here, we incorporated a predisposed point chiral moiety into photoswitches and subsequently amplified supramolecular chirality *via* the coordination-driven self-assembly process. With typical photochromic moieties and the chiral self-assembly strategy, we have successfully set up discrete self-assembled metallacages with the following characteristics: (i) obtaining an ultrahigh photoconversion yield in DTE-based cages, (ii) achieving specific chirality modulation in a remote and non-destructive manner, (iii) demonstrating chiral inequality, supramolecular chirality transfer, and amplification behaviours upon self-assembly process, and (iv) unravelling a stepwise photoisomerization mechanism in a multi-switch system. We reasoned that this coordination-driven self-assembly could provide a promising strategy for organizing photoswitches to

Key Laboratory for Advanced Materials, Joint International Research Laboratory of Precision Chemistry, Molecular Engineering Feringa Nobel Prize Scientist Joint Research Center, Shanghai Key Laboratory of Functional Materials Chemistry, Institute of Fine Chemicals, School of Chemistry and Molecular Engineering, East China University of Science and Technology, 200237, China. E-mail: whzhu@ecust.edu.cn

† Electronic supplementary information (ESI) available. See DOI: https://doi.org/10.1039/d3sc00828b

‡ These authors contributed equally to this work.

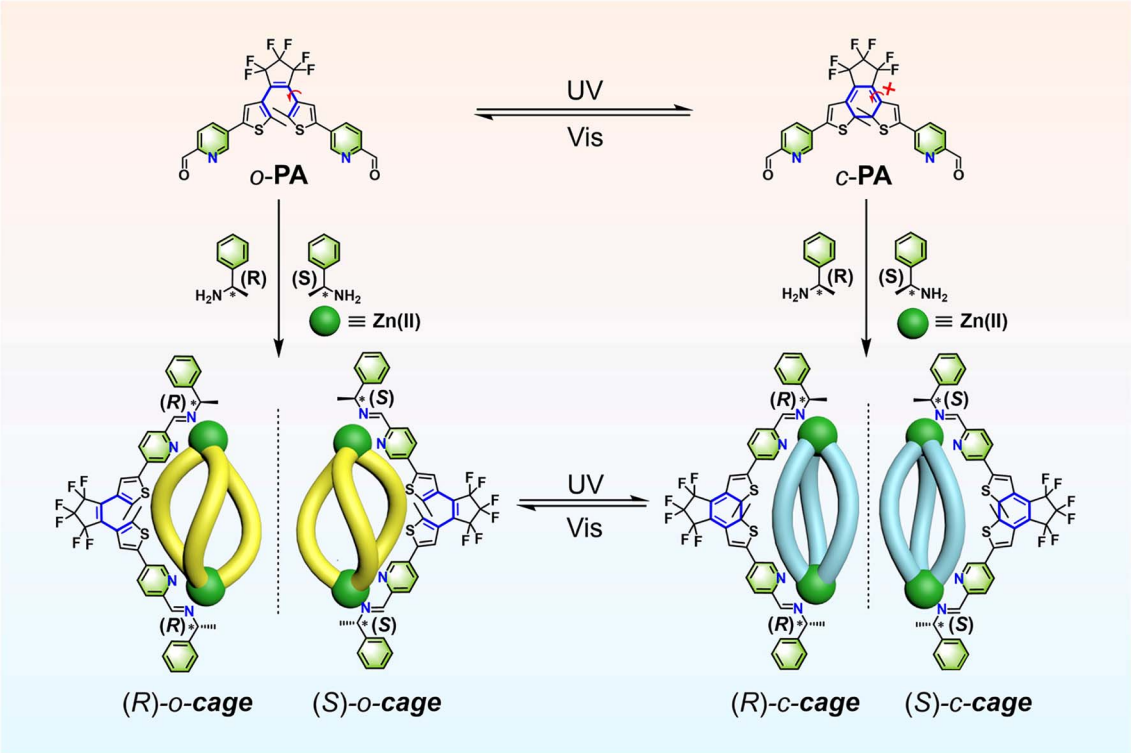

Fig. 1 Self-assembly representation of DTE units, chiral amines, and zinc ions into chiral [3 + 2] metallacages and graphical representation of light-induced transformation between an (*R*/*S*)-*o*-**cage** and (*R*/*S*)-*c*-**cage**.

construct dynamic hierarchical systems for simplifying, understanding, and manipulating chirality at the supramolecular level.

Results and discussion

Self-assembly of dithienylethene photoswitches into metallacages

Ligand *o*-**PA** was synthesized by the Suzuki cross-coupling reaction of dibromo-substituted DTE and picolinaldehyde borate. As illustrated in Scheme S1,† *c*-**PA** was obtained by the ultraviolet (UV) light irradiation of *o*-**PA**. The enantiotropic (*R*/*S*)-*o*-**cage** can be established through a hierarchical self-assembly reaction from ligand *o*-**PA**, (*R*/*S*)-phenylethylamine, and zinc triflate in a molar ratio of 3 : 6 : 2 in acetonitrile at 70 °C for 12 h in a high yield. In fact, this hierarchical self-assembly reaction can be divided into two processes, including the imine condensation reaction between *o*-**PA** and (*R*/*S*)-phenylethylamine, which forms the model ligand *o*-**ML**. And the subsequent metal–ligand coordination between the model ligand and Zn^{2+}, which forms the target chiral metallacages. On the other hand, due to the relatively low thermal stability of *c*-**PA** at 70 °C, we synthesized an (*R*/*S*)-*c*-**cage** at room temperature to prevent undesired thermal cycloreversion reactions. The structures of metallacages were fully characterized by using multinuclear NMR (^{1}H and ^{19}F) spectroscopy, two-dimensional diffusion-ordered ^{1}H NMR spectroscopy (DOSY), and high-resolution electrospray ionization (ESI-HRMS) spectra. In addition, the model ligands *o*/*c*-**ML** were also synthesized for comparing investigations with metallacages, as confirmed by ^{1}H NMR spectroscopy and ESI-HRMS spectra (ESI†).

The formation of single complexes with a high-symmetry structure was revealed by ^{1}H NMR spectra of the *o*-**cage**. After self-assembly, the original aldehyde proton signal at 10.07 ppm disappears while a new signal at 8.07 ppm corresponding to the imine bond appears, which indicates the formation of a pure complex (Fig. S1†). The clear proton splitting of target complexes suggests that multiple DAE units are in an identical chemical environment. This transformation of covalent bonds was verified by FT-IR spectroscopy, showing typical imine bonds at 1638 cm^{-1} instead of aldehyde bonds at 1709 cm^{-1} (Fig. S2†). We further identified every proton through ^{1}H–^{1}H COSY spectra (Fig. S3†). The coordination stoichiometry of metallacages was supported by the ESI-HRMS spectrum (Fig. 2e, S5 and S6†). The results display two peaks at $m/z = 1391.1832$ and $m/z = 877.8164$, corresponding to $[M–2OTf]^{2+}$ and $[M–3OTf]^{3+}$ due to the loss of OTf^- counterions, which displayed experiment isotopic patterns in perfect agreement with the calculated isotopic distributions. No peaks consistent with self-assemblies formed with other stoichiometries are found. The DOSY experiment also supported the formation of a uniform cage structure, suggesting an *o*-**cage** with the same solvodynamic radius of 10.79 Å according to a *D* value of 5.49×10^{-10} m^2 s^{-1} (Fig. S7†). All these results are clearly indicative of the formation of a perfect structure as a [3 + 2] metallacage.

Photoresponsive chiral inequality behavior in metallacages

However, when we checked the ^{1}H NMR spectra of the obtained closed-form cage, extremely complicated proton peak splitting was observed, which makes it difficult to identify the formation of the discrete cage (Fig. S8†). To solve this problem, we adapted an indirect approach to prove the fabrication of the *c*-**cage** by taking photoresponsive advantage of the reversible conversion of the inserted DTE (Fig. 2a). Under visible light (>510 nm) irradiation, the change of the proton signals of the *c*-**cage** in acetonitrile-d_3 solution was monitored by ^{1}H NMR. Interestingly, the proton signals belonging to the *o*-**cage** gradually appeared along with the disappearance of complicated proton signals. Therefore, we proved the formation of the *c*-**cage** in this way (Fig. 2b), and the DOSY experiment suggested a *c*-**cage** with a similar solvodynamic radius of 9.83 Å according to a *D* value of 6.02×10^{-10} m^2 s^{-1} (Fig. S9†). The coordination stoichiometry of the *c*-**cage** was supported by the ESI-HRMS spectrum (Fig. S10–S12†).

In ^{1}H NMR spectra of the *c*-**cage**, we found weird and complicated proton splitting signals. Such an interesting phenomenon could be attributed to the intrinsic chirality of *c*-**PA**. As shown in Fig. 2c, for traditional DTE derivatives, the open-form *o*-**PA** structure was achiral due to the free rotation of the thiophene groups.[13,59] When exposed to UV light, the closed form has a pair of enantiomers with *R* and *S* central chiral conformers. The difference between (*S*,*S*)-*c*-**PA** and (*R*,*R*)-*c*-**PA** enantiomers cannot be observed using ^{1}H NMR spectra. When we employed (*S*)-phenylethylamine-*c*-**PA** to build the (*S*)-phenylethylamine-*c*-**cage**, the complexity of the *c*-**cage** can be attributed to the random self-assembly of *R* and *S* conformers. Here, for example, the (*S*)-phenethylamine-(*RSS*)-*c*-**cage** is depicted as (*S*)-*RSS* for simplicity, thus resulting in four types in stereochemistry: (*S*)-*SSS*, (*S*)-*RRR*, (*S*)-*RSS*, and (*S*)-*RRS*. As depicted in Fig. 2d, (*S*)-*SSS* and (*S*)-*RRR* would not lead to a splitting, as their ligands could be converted into each other *via* rotation around a C_3 axis. However, (*S*)-*RSS* and (*S*)-*RRS* could not convert into each other through any symmetry operation on ligands; *R*- and *S*-ligands would generate two splittings in one cage, which experience different chemical environments. Alternatively, when exposed to the irradiation of visible light, these proton splittings would disappear because of the formation of an achiral open-form state. Depending on this reversible conversion between the

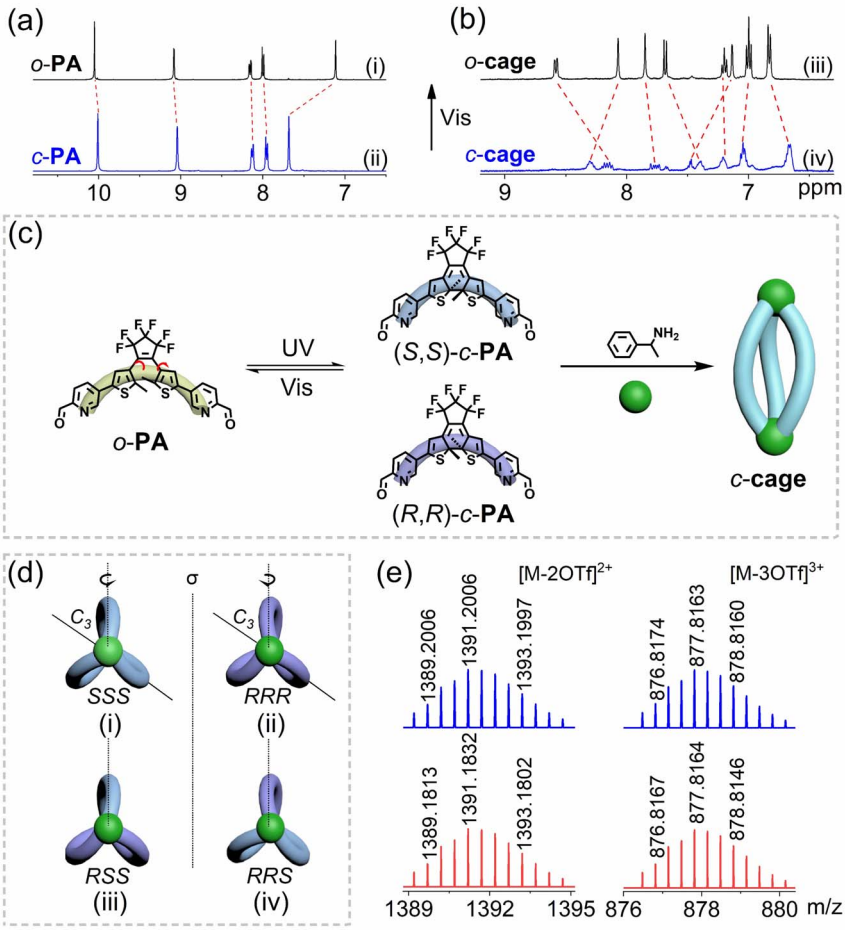

Fig. 2 Photoresponsive chiral inequality behaviour in supramolecular metallacages. (a and b) Partial ^{1}H NMR spectra (400 MHz, CD_3CN, 293 K) of *o*-**PA**, *c*-**PA**, *o*-**cage**, and *c*-**cage**. (c) Graphical representation of the intrinsic chirality of *c*-**PA**. (d) Detailed illustration of the possible isomers of the *c*-**cage** in stereochemistry: *SSS*, *RRR*, *RSS*, and *RRS*. (e) Experimental (red) and calculated (blue) ESI-HRMS spectra of the *o*-**cage**: $[M-2OTf]^{2+}$ (left) and $[M-3OTf]^{3+}$ (right).

open- and closed-DTE ligands, we systemically investigated and explained the chiral inequality phenomenon in self-assembly processes.

Subsequently, density functional theory (DFT) geometry optimizations and calculations are performed to investigate the stability of the above possible isomers (Table S1†). We found three possible isomers: (*S*)-*RRS*, (*S*)-*RSS*, and (*S*)-*SSS* that differ in energy, and their energy relationship is (*S*)-*RRS* > (*S*)-*RSS* > (*S*)-*SSS*, indicating that the (*S*)-*SSS* isomer is more stable than (*S*)-*RRS* and (*S*)-*RSS* in thermodynamics, and the chirality of amine is preferentially induced in the same class of the chiral DTE isomer. To prove this conclusion, we used achiral phenylmethylamine to construct achiral metallacages *o*-**2** and *c*-**2** for comparison, which was confirmed using ^{1}H NMR, ^{13}C NMR, and ESI-HRMS spectra (Fig. S30–S33†). DFT calculations, as shown in Table S2,† reveal that *RRS*, *RSS*, and *SSS* isomers of achiral metallacage have almost equal energy, which demonstrated that the primary factor affecting the stability between chiral configurations is the chirality of the amine, rather than the chirality of DTE itself.

Light-driven supramolecular chirality modulation in metallacages

For multiple-photoswitch systems, the performance of the photoresponsive unit may be affected or locked when other units have a closed-form, due to the gradual formation of high energy barrier of configuration tension. Therefore, achieving a high conversion yield in a nanoconfined framework is challenging. As shown in Fig. 3a, the *o*-**cage** showed two intensive absorption bands at 260 and 325 nm. Compared with free model ligands, the molar extinction coefficient at 325 nm of metallacages displayed a 2-fold enhancement, and a new peak formed at 260 nm, which can be attributed to the increase in ligands and the coordination interaction, respectively. Upon UV light irradiation (313 ± 10 nm), the acetonitrile solution of the *o*-**cage** changed from colourless to blue with an increased broad peak at 450–770 nm, resulting from the large π-conjugated structure of the *c*-**cage**. Inspiringly, we found an ultrahigh photoconversion yield of 91.3% for metallacages, calculated using UV-vis absorption spectra. In addition, the quantum yield of photocyclization for metallacages is 0.356, similar to the free ligands (Table 1). Such high photoconversion performances indicated that the inner responsive units remain relatively independent from each other, which can be attributed to the flexibility of coordination bonds. Alternating irradiation with UV (313 ± 10 nm) and visible light (>510 nm) repeatedly switched the metallacages between ring-open and ring-closed forms, demonstrating remarkable fatigue resistance with no apparent degradation after 10 cycles (Fig. S13c†). Furthermore, these cages displayed excellent thermal stability at both the open state and PSS, showing no obvious decays over 1000 minutes at 298 and 323 K (Fig. S13d and S14†). Similar performances were also found in free model ligands for *o*-**ML** (Fig. S15†). These photochemistry results demonstrated that the photoresponsive metallacages maintain excellent photochromic performance as free ligands, without obvious limitation by frameworks.

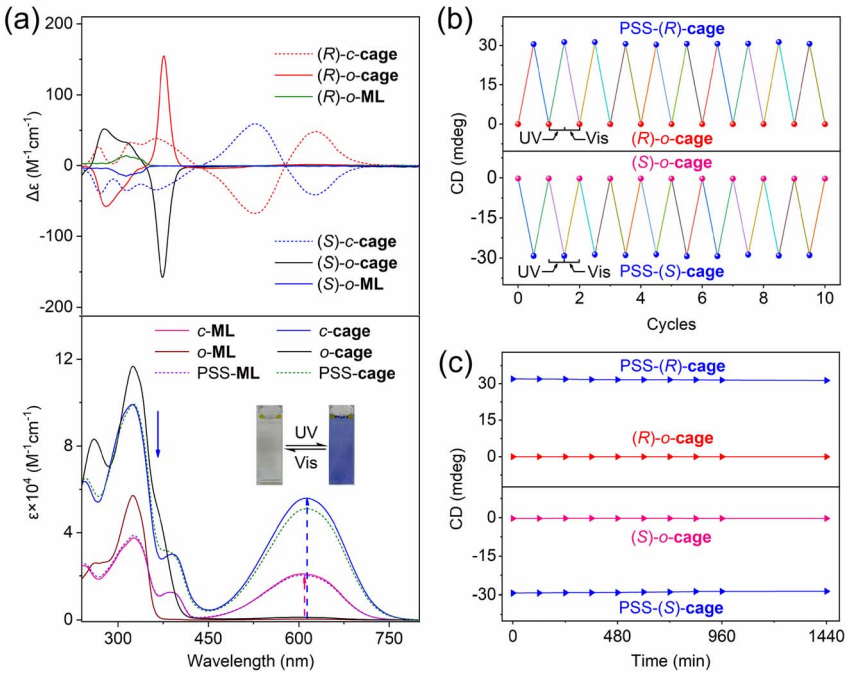

Fig. 3 Photoresponsive chirality amplification in supramolecular metallacages. (a) CD (top) and UV/Vis (bottom) spectra of the (*R*/*S*)-**cage** ($c = 1 \times 10^{-5}$ M) and (*R*/*S*)-**ML** in CH_3CN (3×10^{-5} M). (b) CD spectra of the (*R*/*S*)-**cage** ($\lambda = 630$ nm, $c_{(R)} = 3.4 \times 10^{-5}$ M, $c_{(S)} = 3.3 \times 10^{-5}$ M) in CH_3CN upon irradiation of UV light ($\lambda = 313 \pm 10$ nm) and visible light ($\lambda > 510$ nm), alternatively. (c) Decay curves of the (*R*/*S*)-**cage** ($\lambda = 630$ nm, $c_{(R)} = 3.4 \times 10^{-5}$ M, $c_{(S)} = 3.3 \times 10^{-5}$ M, 298 K) at open- and PSS states upon irradiation of UV light ($\lambda = 313 \pm 10$ nm), monitored at CD absorption.

Table 1 Spectroscopic data of the model ligands and self-assembly metallacages in CH_3CN solution

Compounds	$\lambda_{abs,max}$ [a] (nm) [ε_L [b]/ε_M [b] (10^3 M^{-1} cm^{-1})]	CR_{o-c} [c] [%]	CR_{c-o} [c] [%]	Φ_{o-c} [d] [%]	Φ_{c-o} [d] [%]
***o*-ML**	324 [57.1]	94.1	—	39.2	—
***c*-ML**	608 [62.8]	—	>99	—	0.64
***o*-cage**	326 [38.7/116.1]	91.3	—	35.6	—
***c*-cage**	610 [18.6/55.8]	—	>99	—	0.50

[a] Typical absorption maxima of the ring-open isomer in the UV region and the ring-closed isomer in the visible region, respectively. [b] ε_L represents the molar extinction coefficient of metallacages calculated using the concentration of the ligands and ε_M represents the molar extinction coefficient of metallacages calculated using the concentration of metallacages. [c] Conversion ratio from open to closed isomers (irradiation at $\lambda = 313 \pm 10$ nm) and ring-open isomers (under visible light irradiation, $\lambda > 510$ nm), calculated from absorption spectra. [d] Quantum yields of photocyclization (Φ_{o-c}) at 313 nm and cycloreversion (Φ_{o-c}) at 517 nm.

Circular dichroism (CD) signals originate from the electronic transitions of the chromophore and are generally sensitive to isomerization among distinct conformational states, which is a powerful tool to monitor dynamic chiral conformation changes during light-driven processes.[60,61] As shown in Fig. 3a, the (*R*/*S*)-***o*-cage** in acetonitrile solution exhibited perfect mirror image signals at 250–800 nm, indicative of its enantiomeric nature. Compared with free model ligands (*R*/*S*)-***o*-ML**, the chirality of metallacages showed a 10-fold enhancement, along with a redshift of about 60 nm. These obvious chirality amplification and redshift effects suggested that the chirality transferred from the point chirality of the phenylethylamine to the helix chirality based on the metal coordination. Notably, the (*R*/*S*)-***o*-cage** displayed strong absorption at 250–415 nm, while the (*R*/*S*)-***c*-cage** exhibited two strong absorption peaks at 400–800 nm, along with the characteristic Cotton effects, indicating that the amplification chirality can transfer to the photoswitches and enhance their light-driven chirality regulation capacity. As shown in Fig. 3b, the chirality of metallacages can be modulated with specificity and reversibility. Alternating irradiation with UV (313 ± 10 nm) and visible light (>510 nm) repeatedly switched the metallacages between ring-open and ring-closed forms, demonstrating remarkable fatigue resistance without apparent degradation after 10 cycles. Furthermore, these cages provided excellent thermal stability in both the open state and PSS, showing no obvious decays over 1400 minutes at 298 K (Fig. 3c). This dynamic chiral model with chirality transfer, amplification, induction, and high-efficiency manipulation characteristics is beneficial for understanding and simplifying chirality effects at the supramolecular level.

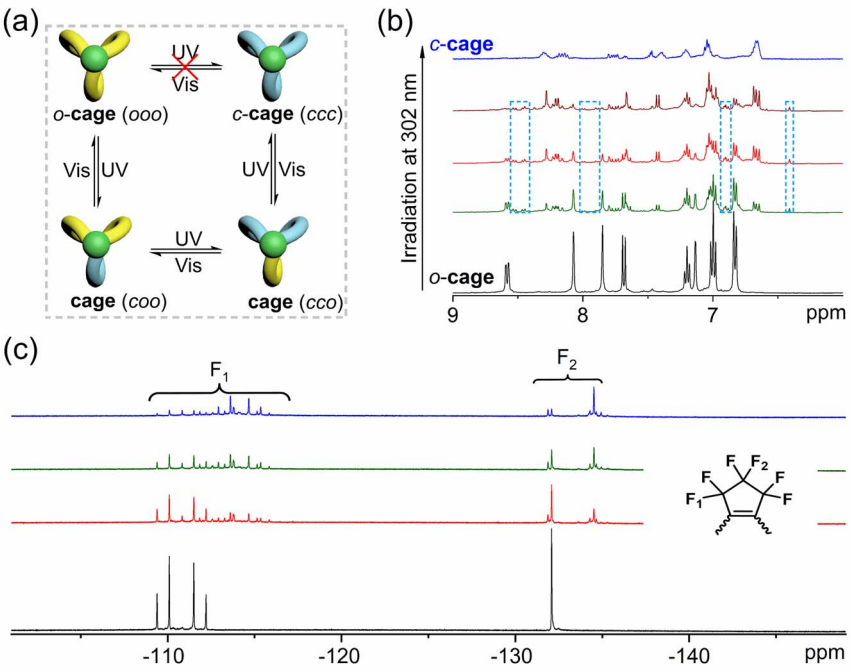

Fig. 4 Photoresponsive supramolecular metallacages self-assembled by stepwise transformation. (a) Graphical representation of the photoconversion of metallacages. (b) Partial ^1H NMR (400 MHz, CD_3CN, 298 K) spectra of the structural photoconversion of metallacages from the ring-open to the ring-closed form upon UV irradiation ($\lambda = 302 \pm 10$ nm). Intermediate states are marked in the blue box. (c) Partial ^{19}F NMR (376 MHz, CD_3CN, 298 K) spectra under the same experimental conditions.

Photo-triggered stepwise transformation of photoresponsive units in metallacages

For this high conversion system, insight into dynamic transformation mechanisms is meaningful for understanding the interaction of inner units. Until now, two different transformation mechanisms have been proposed in self-assembly systems: stepwise transformation,[24] which has experienced *ooc* and *occ* intermediate states and concerted transformation,[38] which has transformed directly from *ooo* to *ccc* without any intermediate (Fig. 4a). To demonstrate this mechanism, we employed ^{1}H and ^{19}F NMR titration experiments to track the transition from an open state to a closed state. As depicted in Fig. 4b, a series of clear proton signals were observed downfield for the initial *o*-**cage**. When exposed to UV light, some intermediate product signals would generate gradually, with no association to the *c*-**cage**. For example, the double peak of the *o*-**cage** at 8.58 ppm turned gradually into two sets of peaks at 8.53 ppm and 8.46 ppm of intermediate products. Unfortunately, due to the complexity of the three possible transformation products (*coo*, *cco*, and *ccc*), we can only distinguish the open (*ooo*) and closed (*ccc*) forms in the ^{1}H NMR spectra, whereas other isomers cannot be identified. Similar results were also displayed in ^{19}F NMR spectra (Fig. 4c), with the initial two sets of fluorine atoms located at −110 ppm and −132 ppm for F_1 and F_2, respectively. When exposed to UV light, we found that there were a lot of intermediate fluorine atom peaks, which are quite complicated to identify. The capture of these intermediate products reveals a step-by-step photoconversion process in photoresponsive metallacages. From the insight of cage tension, the cyclization reaction energy barrier of other units may be increased gradually when one unit has a closed-form. Moreover, 2D exchange spectroscopy (EXSY) experiments on model ligands and metallacages were performed to investigate the existence of metallacage recombination during the isomerization process. As shown in Fig. S20,† we cannot find any exchange cross-peaks between model ligands and metallacages, only imine exchange cross-peaks, which indicated no metallacage recombination in the isomerization process. All the results suggested that our metallacages have broken the isomerization limitation by frameworks, which can be attributed to the rational design of flexible building blocks and the coordination-driven self-assembly strategy.

Conclusions

In summary, we have successfully established a series of dynamic chiral photoswitches based on supramolecular metallacages through coordination-driven self-assembly. Taking photoresponsive advantage of the reversible transformation of DTE between the open- and closed-forms, the chiral inequality phenomenon in metallacages was demonstrated systematically, resulting from the intrinsic chirality of closed-form ligands. More importantly, DTE units loaded on the metallacages could undergo a stepwise photo-triggered isomerization without obvious limitation by frameworks, and achieve an ultrahigh photoconversion yield of 91.3%. Upon such a self-assembly strategy, chirality can conduct transfer and amplification from building blocks to frameworks modulated with DTE photoswitches efficiently. This study provides a dynamic photoregulating chirality platform for building a bridge between small molecules and superstructures to explore more complex chirality mechanisms.

Data availability

All relevant data is presented in the paper and ESI.†

Author contributions

S. Guo and M. Li contributed equally to this work. W.-H. Zhu supervised the study, directed the scientific research, and prepared the manuscript. S. Guo carried out synthesis and conducted UV-vis, NMR, and CD spectroscopy. S. Guo, M. Li and H. Hu conducted the date analysis and wrote the manuscript. All authors discussed the results and edited the manuscript.

Conflicts of interest

There are no conflicts of interest to declare.

Acknowledgements

This work was supported by the NSFC Science Center Program (21788102, 21636002, 22208100 and 22108076), Scientific Committee of Shanghai (21JC1401700 and 15XD1501400), China Postdoctoral Science Foundation (2019M661399, 2021M691006 and 2022M721143) and Shanghai Sailing Program (20YF1410500, 22YF1410400 and 23YF1409000). We thank Prof. Xin-Ping Wu and Mingyu Yang for their help with the DFT calculations.

Notes and references

1 X. Dou, N. Mehwish, C. Zhao, J. Liu, C. Xing and C. Feng, *Acc. Chem. Res.*, 2020, **53**, 852.
2 L. Zhang, H.-X. Wang, S. Li and M. Liu, *Chem. Soc. Rev.*, 2020, **49**, 9095.
3 L.-J. Chen, H.-B. Yang and M. Shionoya, *Chem. Soc. Rev.*, 2017, **46**, 2555.
4 M. Liu, L. Zhang and T. Wang, *Chem. Rev.*, 2015, **115**, 7304.
5 M. Pan, K. Wu, J.-H. Zhang and C.-Y. Su, *Coord. Chem. Rev.*, 2019, **378**, 333.
6 J. Dong, Y. Liu and Y. Cui, *Acc. Chem. Res.*, 2021, **54**, 194.
7 D. Zhao, T. van Leeuwen, J. Cheng and B. L. Feringa, *Nat. Chem.*, 2017, **9**, 250.
8 Y. Sang and M. Liu, *Chem. Sci.*, 2022, **13**, 633.
9 G. Laurent, D. Lacoste and P. Gaspard, *Proc. Natl. Acad. Sci. U. S. A.*, 2021, **118**, e2012741118.
10 Y. Chen, K. Deng, S. Lei, R. Yang, T. Li, Y. Gu, Y. Yang, X. Qiu and C. Wang, *Nat. Commun.*, 2018, **9**, 2711.
11 Q. Sallembien, L. Bouteiller, J. Crassous and M. Raynal, *Chem. Soc. Rev.*, 2022, **51**, 3436.
12 M. Irie, T. Fukaminato, K. Matsuda and S. Kobatake, *Chem. Rev.*, 2014, **114**, 12174.

13 M. Li and W.-H. Zhu, *Acc. Chem. Res.*, 2022, **55**, 3136.
14 C. Jia, A. Migliore, N. Xin, S. Huang, J. Wang, Q. Yang, S. Wang, H. Chen, D. Wang, B. Feng, Z. Liu, G. Zhang, D.-H. Qu, H. Tian, M. A. Ratner, H. Q. Xu, A. Nitzan and X. Guo, *Science*, 2016, **352**, 1443.
15 J. Qi, C. Chen, X. Zhang, X. Hu, S. Ji, R. T. K. Kwok, J. W. Y. Lam, D. Ding and B. Z. Tang, *Nat. Commun.*, 2018, **9**, 1848.
16 J. C.-H. Chan, W. H. Lam, H.-L. Wong, W.-T. Wong and V. W.-W. Yam, *Angew. Chem., Int. Ed.*, 2013, **52**, 11504.
17 X. Meng, W. Zhu, Q. Zhang, Y. Feng, W. Tan and H. Tian, *J. Phys. Chem. B*, 2008, **112**, 15636.
18 S. Becht, R. Sen, S. M. Büllmann, A. Dreuw and A. Jäschke, *Chem. Sci.*, 2021, **12**, 11593.
19 S. Ohshima, M. Morimoto and M. Irie, *Chem. Sci.*, 2015, **6**, 5746.
20 S. Chen, L.-J. Chen, H.-B. Yang, H. Tian and W. Zhu, *J. Am. Chem. Soc.*, 2012, **134**, 13596.
21 Z. Li, X. Liu, G. Wang, B. Li, H. Chen, H. Li and Y. Zhao, *Nat. Commun.*, 2021, **12**, 1363.
22 T. Fukushima, K. Tamaki, A. Isobe, T. Hirose, N. Shimizu, H. Takagi, R. Haruki, S.-I. Adachi, M. J. Hollamby and S. Yagai, *J. Am. Chem. Soc.*, 2021, **143**, 5845.
23 M. Han, R. Michel, B. He, Y.-S. Chen, D. Stalke, M. John and G. H. Clever, *Angew. Chem., Int. Ed.*, 2013, **52**, 1319.
24 R.-J. Li, J. J. Holstein, W. G. Hiller, J. Andréasson and G. H. Clever, *J. Am. Chem. Soc.*, 2019, **141**, 2097.
25 B. J. Furlong and M. J. Katz, *J. Am. Chem. Soc.*, 2017, **139**, 13280.
26 J. Park, D. Feng, S. Yuan and H.-C. Zhou, *Angew. Chem., Int. Ed.*, 2015, **54**, 430.
27 Y. Qin, L.-J. Chen, F. Dong, S.-T. Jiang, G.-Q. Yin, X. Li, Y. Tian and H.-B. Yang, *J. Am. Chem. Soc.*, 2019, **141**, 8943.
28 H.-G. Fu, Y. Chen, X. Y. Dai and Y. Liu, *Adv. Opt. Mater.*, 2020, **8**, 2000220.
29 H. Wu, Y. Chen, X. Dai, P. Li, J. F. Stoddart and Y. Liu, *J. Am. Chem. Soc.*, 2019, **141**, 6583.
30 M. Li, L.-J. Chen, Z. Zhang, Q. Luo, H.-B. Yang, H. Tian and W.-H. Zhu, *Chem. Sci.*, 2019, **10**, 4896.
31 R. J. Li, M. X. Han, J. Tessarolo, J. J. Holstein, J. Lubben, B. Dittrich, C. Volkmann, M. Finze, C. Jenne and G. H. Clever, *ChemPhotoChem*, 2019, **3**, 378–383.
32 Z.-g. Zheng, Y. Li, H. K. Bisoyi, L. Wang, T. J. Bunning and Q. Li, *Nature*, 2016, **531**, 352.
33 Z. Zheng, H. Hu, Z. Zhang, B. Liu, M. Li, D.-H. Qu, H. Tian, W.-H. Zhu and B. L. Feringa, *Nat. Photonics*, 2022, **16**, 226.
34 M. Li, H. Hu, B. Liu, X. Liu, Z.-G. Zheng, H. Tian and W.-H. Zhu, *J. Am. Chem. Soc.*, 2022, **144**, 20773.
35 C. Li, K. Xiong, Y. Chen, C. Fan, Y.-L. Wang, H. Ye and M.-Q. Zhu, *ACS Appl. Mater. Interfaces*, 2020, **12**, 27651.
36 B. Roubinet, M. Weber, H. Shojaei, M. Bates, M. L. Bossi, V. N. Belov, M. Irie and S. W. Hell, *J. Am. Chem. Soc.*, 2017, **139**, 6611.
37 H. Yang, M. Li, C. Li, Q. Luo, M.-Q. Zhu, H. Tian and W.-H. Zhu, *Angew. Chem., Int. Ed.*, 2020, **59**, 8560.
38 M. Li, L.-J. Chen, Y. Cai, Q. Luo, W. Li, H.-B. Yang, H. Tian and W.-H. Zhu, *Chem*, 2019, **5**, 634.
39 Y. Cai, Z. Guo, J. Chen, W. Li, L. Zhong, Y. Gao, L. Jiang, L. Chi, H. Tian and W.-H. Zhu, *J. Am. Chem. Soc.*, 2016, **138**, 2219.
40 N. Sun, C. Wang, B. Yu, H. Wang, L. J. Barbour and J. Jiang, *ACS Appl. Mater. Interfaces*, 2022, **14**, 1519.
41 J.-H. Zhang, H.-P. Wang, L.-Y. Zhang, S.-C. Wei, Z.-W. Wei, M. Pan and C.-Y. Su, *Chem. Sci.*, 2020, **11**, 8885.
42 E. G. Percástegui, T. K. Ronson and J. R. Nitschke, *Chem. Rev.*, 2020, **120**, 13480.
43 Y. Sun, C. Chen, J. Liu and P. J. Stang, *Chem. Soc. Rev.*, 2020, **49**, 3889.
44 C. T. McTernan, J. A. Davies and J. R. Nitschke, *Chem. Rev.*, 2022, **122**, 10393.
45 K. Wu, K. Li, Y.-J. Hou, M. Pan, L.-Y. Zhang, L. Chen and C.-Y. Su, *Nat. Commun.*, 2016, **7**, 10487.
46 J. Jiao, J. Dong, Y. Li and Y. Cui, *Angew. Chem., Int. Ed.*, 2021, **60**, 16568.
47 J. Jiao, C. Tan, Z. Li, Y. Liu, X. Han and Y. Cui, *J. Am. Chem. Soc.*, 2018, **140**, 2251.
48 J. Jiao, Z. Li, Z. Qiao, X. Li, Y. Liu, J. Dong, J. Jiang and Y. Cui, *Nat. Commun.*, 2018, **9**, 4423.
49 W. Danowski, F. Castiglioni, A. S. Sardjan, S. Krause, L. Pfeifer, D. Roke, A. Comotti, W. R. Browne and B. L. Feringa, *J. Am. Chem. Soc.*, 2020, **142**, 9048.
50 Y. Domoto, M. Abe and M. Fujita, *J. Am. Chem. Soc.*, 2021, **143**, 8578.
51 H. Takezawa, K. Shitozawa and M. Fujita, *Nat. Chem.*, 2020, **12**, 574.
52 Y. Fang, J. A. Powell, E. Li, Q. Wang, Z. Perry, A. Kirchon, X. Yang, Z. Xiao, C. Zhu, L. Zhang, F. Huang and H.-C. Zhou, *Chem. Soc. Rev.*, 2019, **48**, 4707.
53 Q.-F. Sun, J. Iwasa, D. Ogawa, Y. Ishido, S. Sato, T. Ozeki, Y. Sei, K. Yamaguchi and M. Fujita, *Science*, 2010, **328**, 1144.
54 J. L. Bolliger, A. M. Belenguer and J. R. Nitschke, *Angew. Chem., Int. Ed.*, 2013, **52**, 7958.
55 X.-Z. Li, C.-B. Tian and Q.-F. Sun, *Chem. Rev.*, 2022, **122**, 6374.
56 M.-C. Tang, L.-K. Li, S.-L. Lai, W.-L. Cheung, M. Ng, C.-Y. Wong, M.-Y. Chan and V. W.-W. Yam, *Angew. Chem., Int. Ed.*, 2020, **59**, 21023.
57 J. J. D. d. Jong, L. N. Lucas, R. M. Kellogg, J. H. v. Esch and B. L. Feringa, *Science*, 2004, **304**, 278.
58 M. Irie, *Chem. Rev.*, 2000, **100**, 1683.
59 W. Li, C. Jiao, X. Li, Y. Xie, K. Nakatani, H. Tian and W. Zhu, *Angew. Chem., Int. Ed.*, 2014, **53**, 4603.
60 G. Pescitelli, L. Di Bari and N. Berova, *Chem. Soc. Rev.*, 2011, **40**, 4603.
61 A. Ozcelik, R. Pereira-Cameselle, N. Poklar Ulrih, A. G. Petrovic and J. L. Alonso-Gómez, *Sensors*, 2020, **20**, 974.